ChemPubSoc Europe

DOI: 10.1002/chem.201303673

CHEMISTRY
A European Journal
Full Paper

Emission Properties | *Very Important Paper*

VIP Monocyclometalated Gold(III) Monoaryl Complexes—A New Class of Triplet Phosphors with Highly Tunable and Efficient Emission Properties

Alexander Szentkuti, Michael Bachmann, Jai Anand Garg, Olivier Blacque, and Koushik Venkatesan*[a]

Abstract: Highly tunable and rich phosphorescent emission properties based on the stable monocyclometalated gold(III) monoaryl structural motif are reported. Monochloro complexes of the type *cis*-[(N^C)Au($C_6H_2(CF_3)_3$)(Cl)] N^C = 2-phenylpyridine (ppy)] (**1**), [N^C = benzo[*h*]quinoline (bzq)] (**2**), [N^C = 2-(5-Methyl-2-thienyl)pyridine (5m-thpy)] (**3**) were successfully prepared in modest to good yields by reacting an excess of 2, 4, 6-tris(trifluoromethyl)phenyl lithium (LiFmes) with the corresponding dichloride complexes *cis*-[(N^C)$AuCl_2$]. Subsequent replacement of the chloride ligand in **1** with strong ligand field strength such as cyanide and terminal alkynes resulted in complexes of the type *cis*-[(ppy)Au(Fmes)(R)] R = CN (**4**), I (**5**), C≡C–C_6H_5 (**6**) and C≡C–$C_6H_4N(C_6H_5)$-*p* (**7**). Single crystal X-ray diffraction studies of all the complexes except **7** were performed to further corroborate their chemical identity. Thermogravimetric analysis (TGA) studies of the uncommon *cis* configured aryl alkyne complex **7** confirmed the high stability of this complex. Detailed photophysical investigations carried out in solution at room temperature, at 77 K (2-MeTHF) in rigidified media, solid state and 5 wt% PMMA revealed the phosphorescent nature of emission in these complexes. Additionally, their behavior was found to be governed based on both the nature of the cyclometalated ligand and the electronic properties of the ancillary ligands. Highly efficient interligand charge transfer in complex **7** provides access to a wide range of emission colors (solvent-dependent) from deep blue to red with phosphorescence emission quantum yield of 30% (441 nm) and 39% (622 nm) in solution and solid state, respectively, and is the highest reported for any Au^{III} complexes. DFT and TDDFT calculations carried out further validated the observations and assignments based on the photophysical experimental findings.

Introduction

Luminescent molecules based on gold(III) complexes have recently gained tremendous significance owing to their potential applications in the field of phosphorescent organic light emitting diodes (PHOLEDs) and photocatalysis.[1] Owing to the huge potential in solid-state lighting and full color display applications, PHOLEDs have gained increased attention over the years. The attractiveness is due to the leveraging of 100% internal quantum efficiency facilitated by the efficient intersystem crossing, which is enabled by the presence of the heavy atom.[2] In contrast to the vast investigations on Ir^{III} and Pt^{II} complexes,[3] exploration into phosphorescent emitters with other metal centers are quite scarce. In particular, gold(III) complexes which are isoelectronic to the Pt^{II} complexes have been less common in spite of the attractive properties such as low toxicity, inertness and its environmentally benign nature.[4] Also, in comparison to the rich luminescent properties of Au^{I} complexes, Au^{III} complexes that display intense luminescence both at room temperature in solution and in solid state are uncommon.[1a,e,i] The lack of large number of luminescent gold(III) complexes can be attributed to the non-radiative excited-state deactivation caused by the low lying d–d states that are energetically close to the potentially emissive intraligand (IL) or metal-to-ligand charge transfer (MLCT) states.[1b] A successful strategy developed by the groups of Yam and Che pertains to the use of strong field ligand such as alkynes and N-heterocyclic carbenes (NHC) with good σ-donating properties in order to decrease the probability for thermal population of non-emissive d–d states.[1a–l,n] Recently, Yam's group demonstrated a maximum external quantum efficiency (EQE) of 11.5% for an OLED device employing biscyclometalated Au^{III} complex as a dopant with an emission quantum yield of 34% (2 wt% PMMA).[1e,i] Aside from this isolated example, there are no reports of Au^{III} complexes having good quantum yields in the solid state.

[a] *A. Szentkuti, M. Bachmann, Dr. J. A. Garg, Dr. O. Blacque, Dr. K. Venkatesan*
Institute of Inorganic Chemistry
University of Zurich
Winterthurerstrasse 190
CH-8057, Zurich (Switzerland)
Fax: (+41) 446356803
E-mail: venkatesan.koushik@aci.uzh.ch

Supporting information for this article is available on the WWW under http://dx.doi.org/10.1002/chem.201303673.

Nearly all of the reported luminescent Au^{III} complexes consist of the biscyclometalated tridentate ligand scaffold in order to avoid molecular distortions. These distortions could lead to symmetry decrease from D_{4h} to D_{2d}, which is known to facilitate non-radiative excited state decay and decrease the stability of organogold(III) complexes, since they readily undergo reductive elimination to give carbon-carbon coupling products and gold(I) species, especially in the presence of light.[4,5] In view to overcome the stability issues, we recently reported the first luminescent bidentate monocyclometalated Au^{III} complexes stabilized by pentafluorophenyl ligands.[6] Following this work, Yam's group and our group independently reported the first examples of luminescent monocyclometalated Au^{III} complexes bearing dialkynes as ancillary ligands in *cis* configuration.[1f,7] We had also shown that functionalized alkynes bearing even one fluorine group showed marked improvements in stability. In comparison to the Au^{III} dialkyne complexes, complexes ligated with pentafluorophenyl ligands were found to be more stable. Although the monocyclometalated complexes provide one additional substitution/coordination site in comparison to the biscyclometalated complexes, the former also shows greater tendency for reductive elimination when two aryl ligands or alkyne ligands are coordinated *cis* to each other due to the highly oxidizing nature of the gold. Despite the considerably improved stability and the luminescent properties of Au^{III} complexes, significant improvements in emission quantum efficiency is still lagging behind the isoelectronic Pt^{II} analogues. A recent study highlights the challenges associated to obtain stable Au^{III} complexes in spite of using a tridentate ligand core.[5a] In order to obtain monocyclometalated Au^{III} complexes with highly tunable emission properties and good emission quantum yields, we have explored a promising strategy in this work that involves the use of 2, 4, 6-tris(trifluoromethyl)phenyl or fluoromesityl (Fmes) as a primary ancillary ligand. The introduction of the ligand into the coordination sphere was thought to result in stable complexes due to the strong electron withdrawing nature of the fluorine atoms in the ligands, which could increase the metal π-back bonding and as a consequence strengthening the gold–carbon bond. In addition the sterical demand and the electronic nature of the ligand should deactivate the Au^{III} center from the substitution of the second chloride ligand upon binding and also Fmes being a strong field ligand would raise the energy of the non-emissive d–d states with respect to the emissive states considerably and render the resulting complexes emissive. This would further allow for the second chloride to be replaced by other secondary ancillary ligands having different ligand field strengths and electronic properties to tailor the emission properties and increase emission efficiency of the complexes.

Herein, we report the synthesis, structural and photophysical investigations of novel monocyclometalated Au^{III} monoaryl complexes that display phosphorescence emission at room temperature in solution, neat solid and in PMMA. The emission wavelength energies were highly tunable depending on the cyclometalating ligand and replacement of the chloride ligand with electronically different ligands such as cyanide and alkynes allowed successfully to achieve good quantum efficiencies. The quantum efficiencies achieved in the solid state and solution at the red and deep blue region, respectively, are among the highest reported for monocylometalated Au^{III} complexes reported until now. To the best of our knowledge, this work also represents the first report of highly stable Au^{III} complexes bearing a monodentate aryl and alkyne ligand *cis* to each other and successful utilization of Au^{III} complex to achieve widely tunable emission properties across the visible spectrum depending on the microenvironment of the complex.

Results and Discussion

Syntheses of complexes

Owing to the successful preparation of Au^{III} diaryl complexes starting from cyclometalated Au^{III} dichlorides by addition of lithiated aryl carbanions,[6] we chose to adopt a similar synthetic strategy to obtain the desired monoaryl complexes. Treatment of the in situ generated FmesLi (6 equiv) with $[(ppy)Au^{III}Cl_2]$ in Et_2O at 45 °C for 24 h gave the corresponding Au^{III} monoarylchloro complex $[(ppy)Au(C_6H_2(CF_3)_3)(Cl)]$ **1** after purification in 77% yield (Scheme 1). Reactions carried out

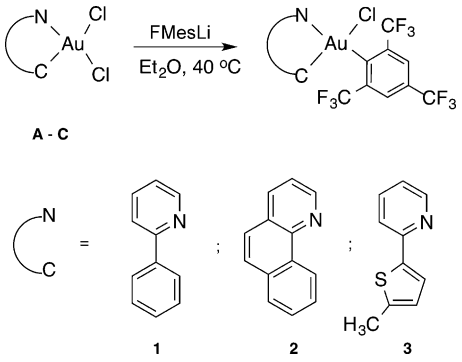

Scheme 1. Synthesis of complexes **1**–**3**.

with less than 6 equivalents of the FmesLi gave lower yields. This finding is consistent with a previous report involving Pd^{II} complexes, where the reaction required excess of FmesLi to achieve the desired product.[8] Our synthetic strategy is different to the previously reported methodology by Tilset and coworkers starting from Au^{III} diacetate.[9]

The ^1H NMR spectrum of complex **1** closely resembled the corresponding starting dichloride complex and displayed only marginal deviations in the chemical shifts along with the presence of an additional new singlet resonance at $\delta = 8.16$ ppm corresponding to the Fmes ligand. The ^{13}C NMR spectrum of **1** revealed a characteristic signal for the quaternary carbon of the Fmes bound to the gold center at $\delta = 143.8$ ppm. The ^{19}F NMR studies gave two singlet resonances corresponding to the *o*-CF_3 and *p*-CF_3 groups at $\delta = -64$ and -61 ppm, respectively, confirming the presence of the Fmes ligand. A single crystal X-ray diffraction study carried out further corroborated the structure of complex **1**. Following similar route as for **1**, but using only 4 equivalents of FmesLi, complexes [(bzq)Au-

$(C_6H_2(CF_3)_3)(Cl)]$ **2** and [(5m-thpy)Au$(C_6H_2(CF_3)_3)(Cl)]$ **3** bearing different cyclometalating ligands were prepared in yields of 32% and 24%, respectively (Scheme 1).

In order to tune the photoluminescence properties of the monocyclometalated Au^{III} monoaryl complexes, the substitution of the chloride with electronically different ligands such as cyanide, iodide and alkyne was sought. These ligands were expected to attenuate the position of the non-emissive metal-centered d–d states due to the different σ-donation properties of the ligands. Treatment of complex **1** with a slight excess of tetrabutylammonium cyanide in CH_2Cl_2 at room temperature for 24 h gave **4** in 92% yield after purification (Scheme 2). The ^{13}C NMR spectrum of **4** in CD_2Cl_2 showed a characteristic resonance at $\delta = 206.8$ ppm for the carbon atom of the cyanide ligand bound to the gold center. The IR spectrum of the compound exhibited a strong stretching vibration at 2164 cm^{-1}.

A single crystal X-ray diffraction study further corroborated the identity of the complex (Figure 1). The complex was found to be stable in air and in common organic solvents for prolonged periods of time and no signs of degradation was observed. While complex (ppy)Au(Fmes)I **5** was easily prepared in 63% yield by treating **1** with NaI in acetone at 40 °C for 24 h (Scheme 2), new reaction protocols were required to achieve complexes **6** and **7**. Our initial attempts to synthesize complex (ppy)Au(Fmes)(C≡C–C_6H_5) **6** directly from **1** by addition of lithium acetylide or by a transmetalation reaction involving copper acetylide in the presence of an amine in CH_2Cl_2 did not result in the expected product. Ag^I phenylacetylide generated in situ by treating trimethylsilyl phenyl acetylene with AgOTf in

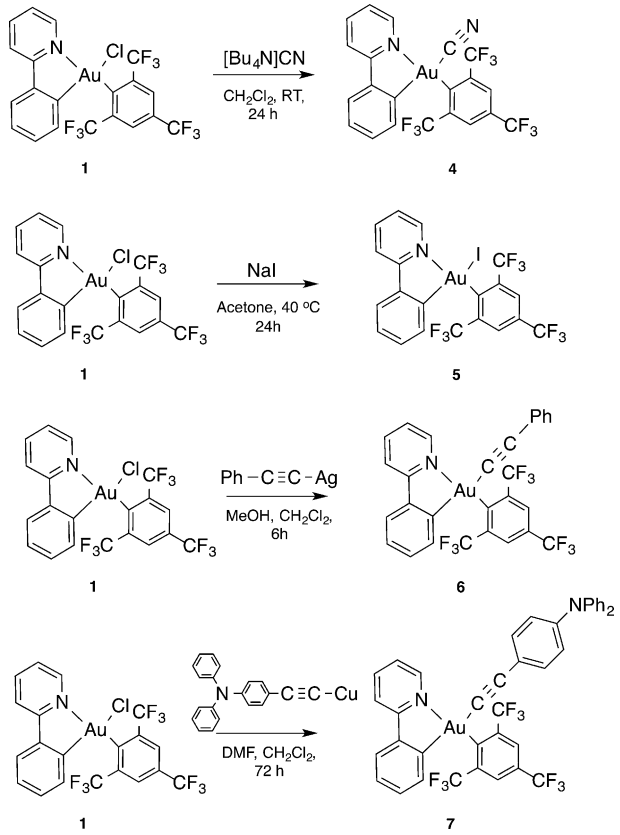

Scheme 2. Synthesis of complexes **4**–**7**.

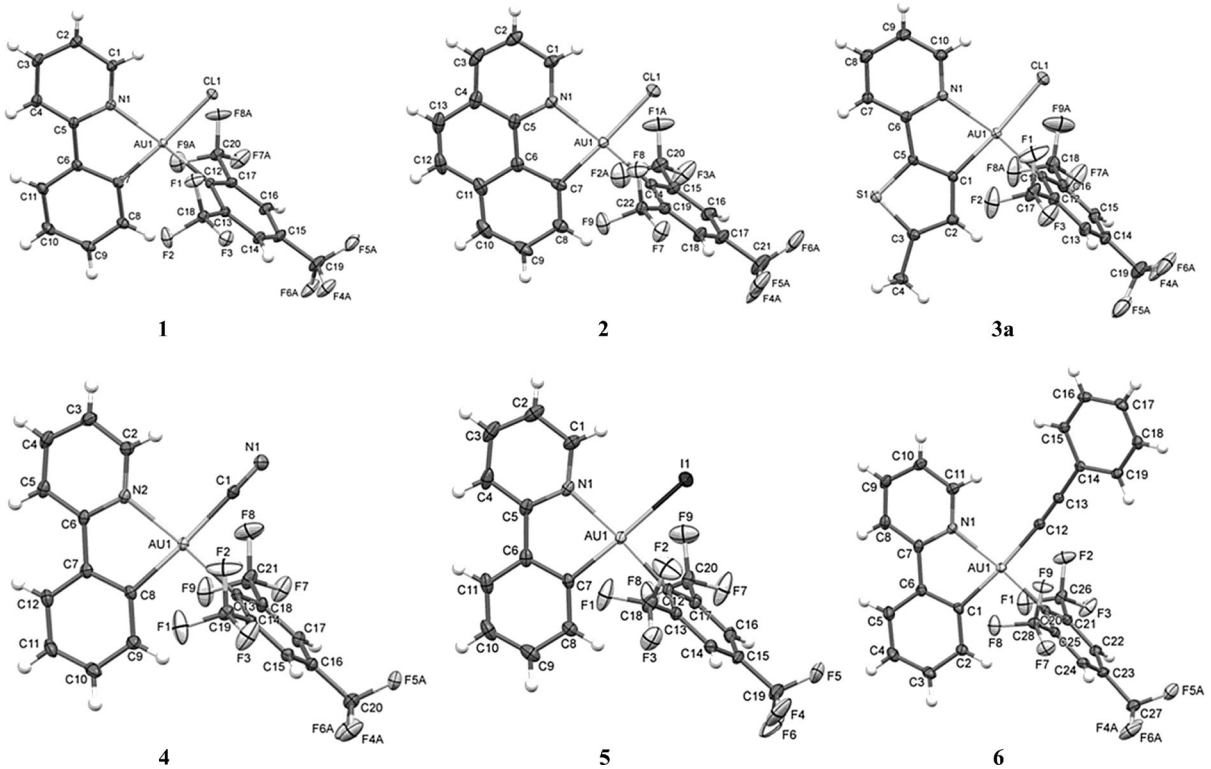

Figure 1. X-ray molecular structures of **1**–**6** with thermal ellipsoids drawn at the 30% probability level. Disorders are omitted for clarity.

MeOH was stirred with complex **1** in CH_2Cl_2 at room temperature (Scheme 2).[10a] Further work-up and purification using column chromatography gave complex **6** in 30% yield. Adopting similar reaction conditions for the preparation of **7** resulted in a dismal yield. However, optimal reaction conditions were successfully obtained by generating in situ the Cu^I acetylide starting from (4-diphenylamino-phenyl)trimethylsilyl alkyne, CsF and CuI in DMF,[10b] which after subsequent treatment with complex **1** in DMF gave the desired complex **7** in 49% yield (Scheme 2). Extensive characterization of complexes **6** and **7** was carried out using ^1H and ^{13}C NMR, 2D NMR studies, elemental analysis and the chemical identity was additionally corroborated for **6** by a single crystal X-ray diffraction analysis. The ^{13}C NMR spectrum in CD_2Cl_2 showed two characteristic resonances at $\delta = 126.2$ and 134.2 ppm for complex **6** that can be attributed to the C_α and C_β of the alkyne bound to the Au^{III} metal center, respectively. Similar resonances were shifted downfield for **7** at $\delta = 115.9$ and 103.5 ppm.

The influence of the different ancillary ligands on thermal stability of the selected complexes **1**, **4** and **7** were evaluated in the solid state using thermogravimetric analysis (TGA) (see Figures S1–S3 in the Supporting Information,). While **4** bearing the cyanide ligand showed the highest stability with the onset of total degradation (T_d) at 300 °C, **1** with the chloride ligand was found to be the least stable with a T_d at 223 °C. Complex **7** has a T_d at 235 °C. An initial weight loss ($T \sim 5\%$) was measured to be 60 °C for complex **1** and 114 °C for both complexes **4** and **7**. These relative stabilities are in accordance with the different kinds of bonding situations of the secondary ancillary ligands to the Au^{III} center.

Structural characterization

X-ray diffraction studies were performed for complexes **1**–**6** with single crystals obtained by slow evaporation of the concentrated solution of the complexes in dichloromethane with a layer of pentane at 0–5 °C. The perspective views of the molecular structures are shown in Figure 1. Table 1 displays selected bond lengths and angles for all structures while the crystallographic details are provided in the Supporting Information. A distorted square planar geometry is observed resulting from the coordination environment around the gold center. This behavior is expected for square-planar d^8 systems with non-equivalent ligands, especially with the constraints of our chelating cyclometalated ligands (N^C). The compound (5m-thpy)AuCl(Fmes) presents two polymorphic crystal structures **3a** (monoclinic, $P2_1/c$) and **3b** (triclinic, $P\bar{1}$), both polymorphs are reported in our manuscript (see the Supporting Information for **3b**). The bond distances Au–N and Au–C_{N^C} were found to lie in the ranges 2.083(2)–2.117(2) Å and 2.004(3)–2.052(3) Å. They are significantly longer than those reported in the X-ray structure of the starting dichloride complex[11] which exhibits values of 2.034(1) and 1.950(2) Å, respectively. The former Au-N distances are also slightly longer than those found for analogous N^C Au^{III} complexes, between 2.052(2) and 2.082(2).[7] The bond distance Au–Cl in complexes **1**–**3** is in the range 2.3384(12)–2.3525 (6) Å. These values are very similar to the one of 2.361(8) Å reported in the dichloride complex, for which a structural *trans* influence was observed for the Au–Cl bond distances (a shorter value of 2.282(5) Å is reported when *trans* to the pyridyl nitrogen). In **1**–**3** the chloride ligand is always *trans* to the Au-C_{N^C} bond and the Au–Cl bond length shows no real deviation with the change of the cyclometalating core. The same observation can be done for the Au–C_{Fmes} bond length which only varies by ± 0.014 Å in **1**–**6**. The Au–$C_{alkynyl}$ bond *trans* to the carbon atom of the pyridyl ring in **6** is 2.039(3) Å and falls in the range of 1.993(2)–2.052(2) Å found for analogous complexes.[7] The bond angle X–Au–C_{Fmes} (X = Cl, C_{CN}, I or C_{CCPh}) is always nearly ideal around 90° in the range 88.12(10)–91.93(12)°, except for **3a** where it is significantly larger with 93.13(8)°. The polymorphic structures **3a** and **3b**, which present significantly different Cl–Au–C_{Fmes} bond angles of 89.25(13) and 93.13(8)° are very good examples to support the evidence that the geometric parameters, especially bond and dihedral angles, have to be considered with care because they can be perturbed by packing forces and intermolecular interactions. The opposite N–Au–C_{N^C} chelate bite angles of the complexes are all smaller than 83.18(12)° (for **2**) while the neighboring C_{N^C}–Au–C_{Fmes} and N–Au–X bond angles are contrarily greater than 92.74(13)° and 94.34(8)°, respectively (except for **3a** for which the former angle is 91.59(11)°; Table 1). The Fmes ligand is almost perpendicular to the chelating metallacycle in each structure. The dihedral angle defined by the mean planes of the N^CAuXC_{Fmes} core and the six-membered ring of the Fmes ligand is in the narrow interval of 88.49(7)-89.43(8)°. For complex **6** the dihedral angle shows a larger deviation from the idealized 90° angle but only by about 5° with 84.97(9)°. The phenyl ring of the alkynyl ligand is almost coplanar with the metallacycle and consequently perpendicular to the Fmes ligand with dihedral angles of 13.1(2) and 74.10(9)° between the mean planes, respectively. The intermolecular Au···Au distances of 6.1874(3) Å for **3b** and 6.2639(4) Å for **4** were found to be the shortest ones among all

Table 1. Selected bond lengths (Å) and angles (°) for **1**–**6**.

	1	2	3a	3b	4	5	6
Au–N	2.083(2)	2.089(2)	2.117(2)	2.103(4)	2.085(2)	2.100(3)	2.086(3)
Au–C_{N^C}	2.019(2)	2.005(3)	2.004(3)	2.005(4)	2.038(3)	2.037(3)	2.052(3)
Au–C_{Fmes}	2.014(2)	2.017(3)	2.019(3)	2.015(4)	2.027(3)	2.028(3)	2.023(3)
Au–X[a]	2.3525(6)	2.3452(8)	2.3414(8)	2.3384(12)	2.045(3)	2.6557(3)	2.039(3)
Au···Au[b]	6.5872(2)	6.8605(2)	7.4738(1)	6.1874(3)	6.2639(4)	7.7450(5)	7.1495(4)
N–Au–C_{N^C}	81.49(9)	83.18(12)	80.89(10)	81.54(17)	80.98(11)	80.95(14)	80.80(12)
C_{N^C}–Au–C_{Fmes}	94.23(10)	93.59(13)	91.59(11)	94.55(18)	93.08(11)	93.99(14)	92.74(13)
C_{Fmes}–Au–X	88.98(7)	88.90(9)	93.13(8)	89.25(13)	90.13(11)	88.12(10)	91.93(12)
X–Au–N	95.30(6)	94.34(8)	94.51(7)	94.63(11)	95.77(10)	96.96(9)	94.65(12)

[a] X = Cl (**1**–**3b**), C_{CN} (**4**), I (**5**) or C_{CCPh} (**6**). [b] Shortest Au···Au distance in the crystal structure.

Table 2. Photophysical data for complexes **1**–**7**.

Complex	Absorption	Medium (T [K])	Emission λ_{max} [nm] (τ_0 [μs])	φ_{em} [%]	k_r $[s^{-1}]\times10^3$	k_{nr} $[s^{-1}]\times10^5$
1	319 (8760)	CH_2Cl_2 (298)	456, 488, 515 (0.49)	0.4	8.2	20.3
		glass (77)	452, 485, 513 (0.64)	–		
		solid (298)	456, 489, 516	4.2		
		PMMA (298)	456, 488	23		
2	340 (1760),	CH_2Cl_2 (298)	464, 497, 533 (0.53)	0.86	16.2	18.7
	355 (3140),	glass (77)	464, 472, 497 (0.63)	–		
	372 (3640)	solid (298)	[a]	[a]		
		PMMA (298)	[a]	[a]		
3	291 (13360),	CH_2Cl_2 (298)	557, 588 (0.93)	0.49	5.3	10.7
	369 (8820)	glass (77)	537, 582, 636 (0.62)	–		
		solid (298)	[a]	[a]		
		PMMA (298)	544, 589	8.5		
4	323 (8960)	CH_2Cl_2 (298)	459, 493, 520 (2.25)	7.49	33.3	4.1
		glass (77)	454, 478, 523 (0.61)	20		
		solid (298)	458, 490, 521	12		
		PMMA (298)	460, 490			
5	310 (8485)	CH_2Cl_2 (298)	456, 488, 517 (0.17)	2.18	128.2	57.5
		glass (77)	453, 486 (0.50)	–		
		solid (298)	[a]	[a]		
		PMMA (298)	[a]	[a]		
6	316 (9800)	CH_2Cl_2 (298)	458, 490, 519 (2.23)	1.07	4.8	4.4
		glass (77)	454, 484, 516 (0.61)	–		
		solid (298)	456, 488, 518	7		
		PMMA (298)	454, 487	28		
7	323 (44600)	CH_2Cl_2 (298)	612 (0.90)	10.0	67.8	10.4
		glass (77)	421, 464, 485 (0.53)	–		
		solid (298)	620, 649	39		
		PMMA (298)	523	14		

[a] Very weak emission.

complexes, the other distances lie between 6.5872(2) and 7.7450(5) Å. Any significant aurophilic interactions could be ruled out, since the Au···Au distances are not shorter than the sum of the van der Waals radii between the gold atoms in the crystal lattices. Again, it is interesting to report the difference between the polymorphic structures of (5m-thpy)AuCl(Fmes) with Au···Au distances of 6.1874(3) Å for **3b** and 7.4738(1) Å for **3a**.

UV/Vis absorption studies

The photophysical data for the complexes are summarized in Table 2. The UV/Vis profiles of complexes **1**–**3** are shown in Figure 2. The shape of the bands closely resembled to those of the respective free ligands, but with strong bathochromic shifts. While complex **1** exhibits a low-energy absorption maxima at 319 nm, complexes **2** and **3** feature bands that are more red shifted to 372 and 369 nm, respectively (Table 2). These shifts are caused due to the internal charge transfer and the increased π-delocalized nature of the cyclometalating ligand of the respective complexes.[3a] The complexes possess molar extinction coefficients in the order of 10^3–10^4 $dm^3 mol^{-1} cm^{-1}$. Substitution of the ancillary chloride ligand in **1** had varying effect on the absorption maxima of the corresponding substituted complexes **4**–**7**. This behavior is in contrast to our previously reported diaryl complexes, where no change was observed with electronically different aryl ligands.[6,7] The UV/Vis profiles of **4**, **5** and **6** are shown in Figure 3. While complex **4** has its absorption maxima at 323 nm, complexes **5** and **6** display a hypsochromic shift of the absorption band to 310 nm and 316 nm, respectively. **7** has bathochromically shifted absorption maximum in comparison to **6** which is consistent with the electron donating substituent on the alkyne. The UV/Vis of **7** measured in solvents of different polarity revealed a hypsochromic shift of 4 nm on going from tetrahydrofuran to cyclohexane. This is indicative

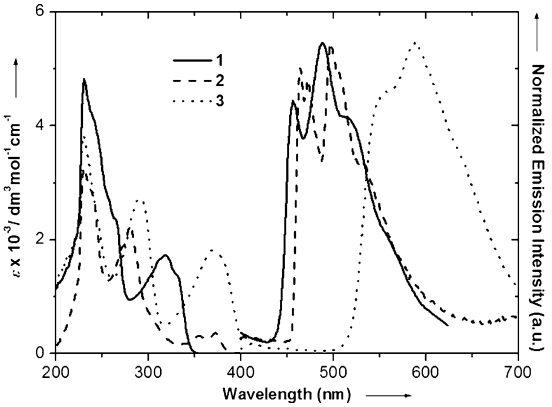

Figure 2. Electronic absorption spectra in CH_2Cl_2 at room temperature and normalized emission spectra of **1**–**3** in degassed CH_2Cl_2 at room temperature.

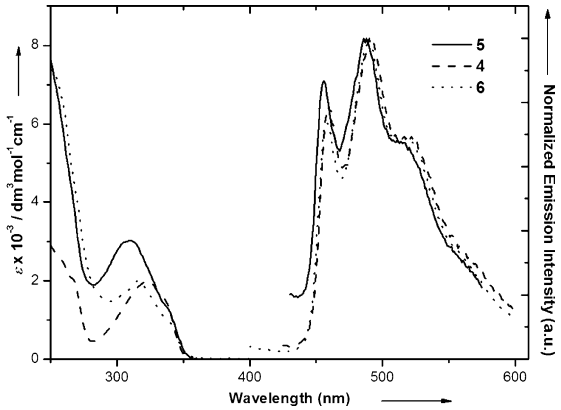

Figure 3. Electronic absorption spectra in CH_2Cl_2 at room temperature and normalized emission spectra of complexes **4**–**6** in degassed CH_2Cl_2 at room temperature.

of a less polar nature of the ground state with respect to the excited state.

Emission studies

Complexes **1**–**7** showed an intense long-lived phosphorescence emission, both at room temperature in CH_2Cl_2 (Figure 2 and 3) and at 77 K (2-MeTHF) rigidified media (Figures S5 and S6 in the Supporting Information). While complexes **1** and **2** bearing ppy and bzq as the cyclometalating ligands displayed a low vibronic structured emission band at similar wavelengths at 488 nm and 497 nm, respectively, complex **3** ligated with the 5m-thpy cyclometalated core displayed the band at a more redshifted wavelength of 588 nm (Table 2). These differences in the emission maxima can be attributed to be arising from different π–π^* energies of the different cyclometalating ligands, which is indicative of the strong participation of the cyclometalate in the excited state. In very much akin to the isoelectronic cyclometalated Pt^{II}, this behavior of the Au^{III} complexes offers an effective way to tailor the desired emission energies by using cyclometalated ligands with varying π–π^* energies. The vibrationally structured emission profiles of complexes **1**–**3** at room temperature coupled with lower microsecond range excited-state lifetime and the low radiative rate constant is strongly suggestive of the origin of the emission to be a predominantly intraligand charge transfer (^{3}ILCT) parentage. The excited-state lifetime of these complexes in the lower micro second range along with the large Stokes shifts and quenching of the emission under aerobic conditions confirms the phosphorescent nature of the emission in complexes **1**–**3**.

The emission wavelength maxima for complexes **4**–**6** in CH_2Cl_2 showed a negligible shift, however, a significant change both in the emission profile and emission wavelength maxima was observed in the case of complex **7**. The photophysical properties of **7** are discussed separately in detail. While **4** has its emission wavelength maximum at 493 nm, for complexes **5** and **6** it was found at 488 nm and 490 nm, respectively. The similar range of the emission wavelength maxima is suggestive of emission origin from a common parentage. The Stokes shifts for the three complexes were in a range between 170 to 178 nm. It can also be estimated that their energy band gap π–π^* is similar to each other. Although the preliminary photophysical measurements point to the lesser role of the ancillary ligands such as chloride, cyanide, iodide and phenylacetylene on the photoluminescence properties, the electronic properties of the ancillary ligands influence on the quantum efficiency in the solid state is very significant and is quite varying. The nature of the emission profiles of **4**, **5** and **6** at room temperature suggests a predominant intraligand charge transfer (^{3}ILCT) character.

Since complex **7** displayed a different emission behavior in comparison to **4**, **5**, and **6**, the influence of the different media on the emission behavior was deeply investigated. Table 3 summarizes the photophysical properties of **7**. The UV/Vis absorption spectrum of **7** in dichloromethane at room temperature shows the low-energy absorption maximum at 323 nm and is similar to the other three complexes due to the same cyclometalating core (Figure 4). Interestingly, complex **7** in dichloromethane at room temperature displayed a broad structureless emission band at 612 nm (Figure 4). The emission profile is significantly shifted to lower energy in comparison to **6**, which also shows a well-structured emission band like the rest of the complexes. The emission at 612 nm for **7** is a consequence of the origin of the nature of the emission comprising of a ligand-to-ligand charge transfer ^{3}LLCT[π(C≡C–

Table 3. Photophysical properties of complex **7** at room temperature.

Medium	Absorption λ_{max} [nm]	Emission λ_{max} [nm]	τ [μs]	φ_p [%]
cyclohexane	329	441	1.25	30
toluene	329	518	0.42	24
DCM	323	612	0.90	10
THF	323	615	1.51	8
solid	334	622	–	39
PMMA 5%	334	494	–	14
PMMA 25%	334	501	–	16
PMMA 50%	334	511	–	21
PMMA 75%	334	523	–	26

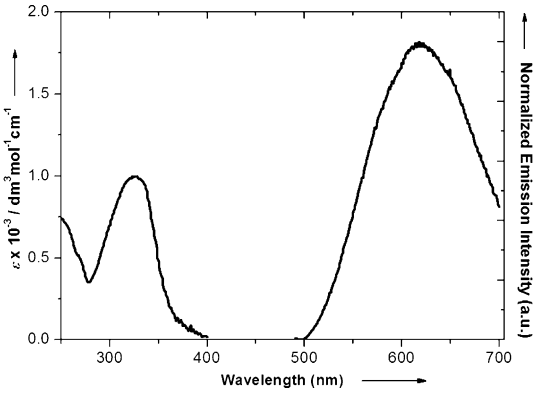

Figure 4. Electronic absorption spectra in CH_2Cl_2 at room temperature and normalized emission spectra of complex 7 in degassed CH_2Cl_2 at room temperature.

$C_6H_4N(C_6H_5)_2$-*p*)→π*(ppy)] from the alkyne ligand to the cyclometalating ligand due to the presence of the energetically higher lying orbital π(C≡C–$C_6H_4N(C_6H_5)_2$-*p*) resulting from the strongly electron donating alkynyl ligand. This assignment is consistent with the results from the DFT and TDDFT calculations. This photophysical behavior of **7** is in contrast to what is found for complexes **4**–**6** where the origin of the emission is assigned to an intraligand charge transfer (^{3}ILCT) centered on the cyclometalating ligand.

As depicted in Figure 5 and Table 3, emission from **7** was found to be significantly dependent on the polarity of the solvent. As the emission excitation spectra are obtained in each

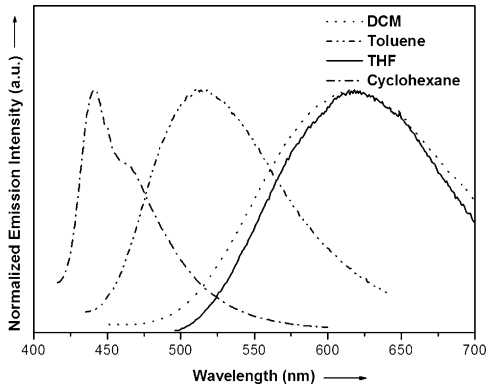

Figure 5. Normalized emission spectra of **7** in cyclohexane, toluene, dichloromethane and tetrahydrofuran at room temperature.

solvent for the wavelengths monitored (450–700 nm), it can be ascertained that the emission band originates from a common ground state species. Furthermore, the excitation spectra, within experimental error, are also effectively identical to the absorption spectra, indicating that the entire phosphorescence results from a common Franck–Condon excited state. Since the absorption peak wavelength exhibits only a slight shift from cyclohexane to tetrahydrofuran, the anomalously large red shifted phosphorescence observed for complex **7** should be attributed to a large change in the dipolar vector of the T_1 state, such that solvent dipolar relaxation takes place during the T_1–S_0 transition, resulting in a distinctive phosphorescence solvatochromism.

We used the Lippert–Mataga equation[12] to quantify the change in dipole moment related to the solvent polarity:

$$\nu_A - \nu_F = \frac{2(\mu_E - \mu_G)^2}{hc\alpha^3}\left(\frac{\varepsilon - 1}{2\varepsilon + 1} - \frac{n^2 - 1}{2n^2 + 1}\right)$$

$$\Delta f = \frac{\varepsilon - 1}{2\varepsilon + 1} - \frac{n^2 - 1}{2n^2 + 1}$$

where ν_A and ν_F are the wavenumbers of the absorption and emission, respectively, μ_E and μ_G are the dipole moments of the molecule in the excited state and ground state, respectively, h is the Planck's constant, c is the speed of light, α is the approximate radius of the cavity in which the molecule resides, ε is the dielectric constant of the solvent and n is the refractive index of the solvent. In this equation, the term Δf is called the orientation polarizability. From the absorption and emission wavelengths recorded for **7** at room temperature in cyclohexane, toluene, dichloromethane and tetrahydrofurane (Table 3), the solvent dependence was estimated by a Lippert plot of ν_A–ν_F vs. the orientation polarizability Δf. Despite the little amount of data, a linear regression gave a slope of 25.8× 10^3 cm^{-1} corresponding to a value of μ_E-μ_G of 27.8 Debye (Figure S25 in the Supporting Information).

In stark contrast to the isoelectronic Pt^{II} complexes,[13] the comparison studies of luminescence properties of Au^{III} complexes both in solution and solid state are scarce.[1e,i] In order to systematically evaluate the influence of the ancillary ligand on the emission properties and emission quantum yields, emission properties of the complexes **1**–**7** were investigated both in neat solid and as 5 wt% of the complex in PMMA film (the emission profiles are illustrated in Figure 6 and Figures S8 and

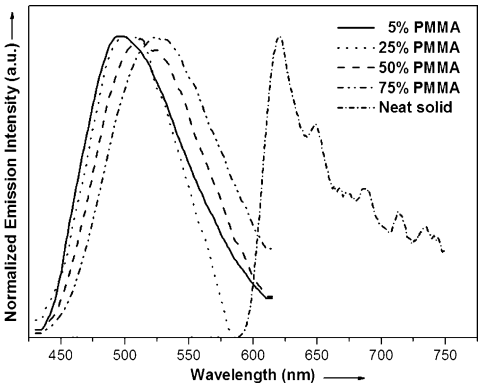

Figure 6. Normalized emission spectra of **7** at different concentrations (wt%) in PMMA films and neat solid at 298 K.

S9 in the Supporting Information). While complexes **2**, **3**, and **5** were found to possess weak to no luminescence in the neat solid, complexes **1**, **4**, **6**, and **7** display modest to good intensity of luminescence and their emission profiles closely resembled the emission spectra in solution. While the emission wavelength maxima in the neat solid for **1** was the same as in solution, complexes **4** and **6** displayed a negligible blueshift of **1** and **2** nm at 459 and 458 nm, respectively, attributable to the rigidochromic effect. In contrast, **7** displayed an emission maximum with a red shift of around 8 nm at 620 nm in comparison to solution. Measurements of absolute quantum yield revealed a high quantum yield of 39% for **7**, while complexes **1**, **4** and **6** possesses 4%, 20% and 7%, respectively. The quantum yield for **7** is the highest reported for a Au^{III} complex in the solid state. Complexes **1**–**7** were also investigated as thin films prepared by spin coating a 5 wt% of complexes in PMMA dissolved in CH_2Cl_2. Similar to their behavior in neat solid, complexes **2** and **5** displayed only a very weak emission, while complex **3** has a quantum yield of 8% with the emission wavelength maxima considerably blueshifted with respect to emis-

sion in solution. Comparison of the emission wavelength maxima of the complexes in 5 wt% PMMA and their emission maxima in CH_2Cl_2 revealed a small rigidochromic shift of 4 nm for **1** and 5 nm for **4** and **6**. A significant hypsochromic shift of around 118 nm was observed in the case of complex **7** in comparison to the emission maxima found for **7** in solution. This significant shift can be attributed due to complex being enveloped in a non-polar medium such as PMMA, which is more comparable to the emission maximum of **7** in toluene. This hypsochromic shift was found to decrease with increasing wt% of the complex in PMMA. Going from 5 to 75 wt%, a difference of around 89 nm was observed between the emission maxima in PMMA and in solution. This shift in the emission maxima based on the different concentrations can arise probably due to excimeric emission resulting from π-stacking of molecules, which increases further with the dial up in concentration. While high quantum yields of 28 and 23% were obtained for complexes **6** and **1** respectively, complex **4** gave a quantum yield of 12%. Similar to the observation of emission maxima dependence on concentration of complex **7** in PMMA, the emission quantum yield for **7** was also found to be concentration dependent. Quantum yields of 26, 21, 16 and 14% were obtained for 75, 20, 25, and 5 wt%, respectively.

Cyclic voltammetry studies

Cyclic voltammetry for all complexes except **2**, **6**, and **7** showed irreversible oxidation peaks in the range from +0.40 to +0.71 V (vs. $Fc^{0/+}$ couple) in DMF at room temperature (Table 4). While no oxidation peaks were observed for **2** and **6** in the scanned range, complex **7** displayed a quasi-reversible oxidation couple at +0.46 V (Figure 7). All complexes showed irreversible cathodic peak potentials in the range from −1.82 to −2.17 V (vs. $Fc^{0/+}$ couple). Both the oxidation and the reduction processes can be assigned to ligand centered electrochemical events consistent with the DFT and TDDFT calculations. The observed trends of the reduction potentials of the complexes bearing the same cyclometalate are suggestive of the reduction process to originate from the cyclometalated part of the complex and the oxidation from the aryl or the alkyne ligand.[1c,d,6,7] Based on the previous CV studies of related complexes and due to the oxidizing nature of the gold(III) complexes, the metal is unlikely to be involved in the redox process.[1c,d] The absence of metal based redox activity and the large electrochemical band gap with the widely separated oxidation and reduction peaks is in line with the observed emission properties whose origin is ligand centered with very limited metal perturbation.

Table 4. Summary of cyclic voltammetry for complexes 1–7 in 0.1 M $[n\text{Bu}_4\text{N}][\text{PF}_6]$ (Au electrode; E vs. $Fc^{0/+}$; scan rate = 100 mV s^{-1}; 20 °C, DMF).

Complex	Oxidation $E_{p,a}$ [V]	Reduction $E_{p,c}$ [V]
1	0.71	−1.82
2	–	−1.73
3	0.40	−1.92
4	0.54	−1.83
5	0.50	−1.81
6	–	−1.92
7	0.46 ($\Delta E_{1/2}$)	−2.17

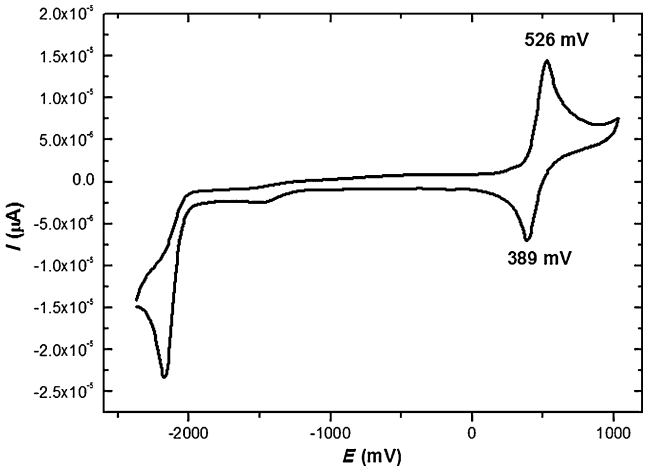

Figure 7. Cyclic voltammogram of **7** in DMF (0.1 M $[n\text{Bu}_4\text{N}][\text{PF}_6]$).

Theoretical calculations

The absorption and emission properties of our series of compounds were investigated by density functional theory (DFT) calculations using the Gaussian 03 program package.[14] The hybrid functional PBE1PBE[15] in conjunction with the Stuttgart/Dresden effective core potentials (SDD) basis set[16] for the Au center augmented with one f-polarization function ($\alpha = 1.050$) and the standard 6-31+G(d) basis set[17] for the remaining atoms was applied. The molecular structures of the electronic ground states and lowest triplet states of the selected compounds **1**–**4** and **6**–**7** were exemplarily studied. On the basis of the ground-state optimized geometries, time-dependent DFT (TD-DFT) calculations[18] combined with the conductive polarizable continuum model (CPCM)[19] were used to produce the ten lowest singlet–singlet and singlet–triplet vertical excitations in the dichloromethane media with the corresponding energies, transition coefficients, and oscillator strengths (Table 5) and the molecular orbital energy levels and compositions (Tables S1 and S2 in the Supporting Information). Full geometry optimizations without symmetry constraints were carried out in the gas phase for the singlet ground states (S_0) and the lowest triplet states (T_1). The optimized geometries S_0 and T_1 were confirmed to be potential energy minima by vibrational frequency calculations at the same level of theory, as no imaginary frequency was found. The lowest-energy absorption maximum of the complexes containing the chelating phenylpyridine ligand ppy (**1**, **4**–**7**) appears in the narrow range 309–323 nm in dichloromethane at room temperature, irrespective of the ancillary Cl, CN, I, C≡CPh or $C{\equiv}CC_6H_4NPh_2$ ligands. Complexes **2** and **3**, which contain different cyclometalated ligands as benzo[*h*]quinoline (bzq) and 2-(5-methyl-2-thienyl)(5m-thpy), feature a more redshifted maximum at 372 and

Table 5. Selected singlet–singlet (S_0–S_n) and singlet–triplet (S_0–T_m) excited states with TD-DFT/CPCM (in dichloromethane) vertical excitation energies (nm), transition coefficients, orbitals involved in the transitions, and oscillator strengths *f* for compounds **1**–**4** and **6**–**7** (with $f > 0.07$).

	1	**2**	**3**	**4**	**6**	**7**
exptl abs., λ_{max}[a]	319	340, 355, 372	291, 369	323	319	323
S_0–S_n	$n=1$	$n=1$	$n=1$	$n=1$	$n=2$	$n=2$
	307.1 (0.235)	339.3 (0.106)	352.0 (0.277)	311.7 (0.242)	316.2 (0.160)	360.4 (0.163)
	HOMO→LUMO (0.66)	H→L (0.67)	H→L (0.65)	H→L (0.66)	H-1→L (0.67)	H→L+1 (0.50)
						H→L+2 (0.44)
	$n=3$	$n=4$	$n=4$	$n=2$	$n=4$	$n=4$
	282.5 (0.096)	277.4 (0.322)	284.0 (0.088)	286.0 (0.086)	291.4 (0.232)	348.5 (0.629)
	H-1→LUMO (0.64)	H→L+2 (0.54)	H→L+1 (0.55)	H-1→L (0.65)	H-2→L (0.64)	H→L+4 (0.62)
		H-1→L (0.33)				
	$n=5$	$n=7$	$n=5$	$n=4$	$n=7$	$n=7$
	267.8 (0.160)	268.1 (0.126)	279.3 (0.153)	256.6 (0.202)	282.2 (0.220)	327.0 (0.077)
	H→L+4 (0.41)	H-1→L+2 (0.52)	H-1→L (0.54)	H→L+3 (0.47)	H→L+4 (0.66)	H-2→L (0.57)
	H→L+4 (0.26)	H→L+5 (0.26)	H→L+4 (0.37)			
		$n=8$	$n=6$		$n=8$	$n=8$
		264.9 (0.082)	279.0 (0.091)		271.6 (0.075)	325.7 (0.231)
		H→L+4 (0.62)	H-1→L (0.39)		H-4→L (0.66)	H-2→L (0.57)
						$n=9$
						321.0 (0.197)
						H→L+2 (0.54)
						H-2→L (0.32)
exptl em., λ_{max}[a]	488	497	588	493	490	494[c]
calcd em., λ_{max}[b]	467 (2.66 eV)	492 (2.52 eV)	586 (2.12 eV)	472 (2.63 eV)	469 (2.65 eV)	490[d] (2.53 eV)
T_1–S_0	437.1	468.0	530.6	440.8	439.7	468.0
	H←LUMO (0.690)	H←L+2 (0.604)	H←L (0.751)	H←L (0.694)	H-1←L (0.632)	H←L+4 (0.531)
						H←L+5 (0.432)

[a] Recorded at room temperature solution in CH_2Cl_2. [b] Calculated as the energy difference between the DFT optimized ground state and triplet state. [c] Recorded in 5 wt% PMMA film. [d] TD-DFT calculations without zero-point correction.

369 nm, respectively, showing the influence of the increased π-delocalized nature of the chelate on the absorption properties. Despite the fact that the PBE1PBE//SDD/6-31+G(d) calculations systematically provide underestimated absorption maxima (by approximately 10–20 nm in our previous studies),[6,7,20] the lowest significant TD-DFT calculated singlet–singlet transitions $S_0 \rightarrow S_1$ for **1**–**4** and $S_0 \rightarrow S_2$ for **6** (the oscillator strength of $S_0 \rightarrow S_1$ being very small, $f = 0.0004$) at 307, 339, 352, 312, 316 nm, respectively, are in a good agreement with the experimental data (average error = 2.6%, maximum error = 4.6% for **3**) and reflect very well the redshift observed for **2** and **3** (Table 5). The $S_0 \rightarrow S_1$ and $S_0 \rightarrow S_2$ transitions derive mainly from the one-electron excitations HOMO→LUMO for **1**–**4** and HOMO−1→LUMO for **6**. The electron density in these frontier orbitals is largely located on the metallacycle N^C ligand (Figure 8) with 93–98% composition and a little participation of the metal, smaller than 5% (Tables S1 and S2 in the Supporting Information). Only the HOMO-1 of **6** shows a significant contribution of the ancillary alkynyl ligand of 16% reducing the participation of the N^C chelate to 80%. Based on these considerations, the lowest-energy absorption band observed in the UV/Vis spectra of our complexes **1**–**6** exhibit an intraligand ^{1}ILCT($\pi_{N^C} \rightarrow \pi^*_{N^C}$) character. Concerning **7** the TD-DFT calculated singlet–singlet transitions $S_0 \rightarrow S_2$ and $S_0 \rightarrow S_4$ at 360 nm (f=0.163) and 348 nm ($f = 0.629$) should be responsible of the absorption band observed at 323 nm. Since, there is large overestimation of the wavelength maxima, the results were dealt with caution. Furthermore, the numerous orbitals involved in the transitions (HOMO, LUMO+1, LUMO+4, LUMO+5) and their various shapes (Figure 8, Figure S15 in the Supporting Information) do not allow us to give a clear assignment of the redshifted band.

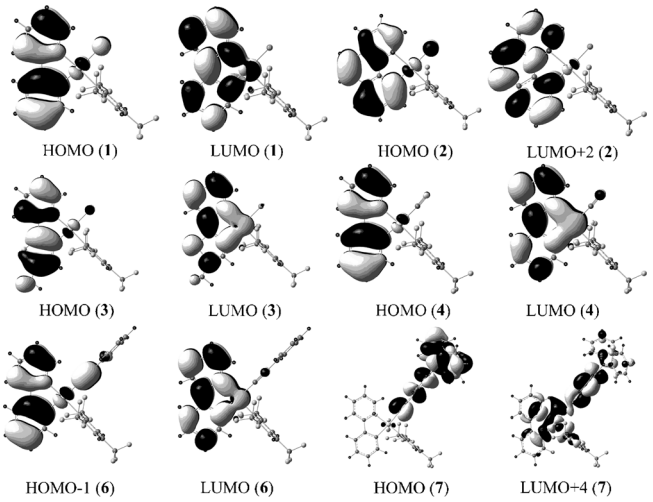

Figure 8. Spatial plots of selected frontier orbitals of the optimized ground states of **1**–**4** and **6**–**7**.

The lowest singlet–triplet vertical excitation (T_1–S_0) energies obtained by TD-DFT on the ground state structures are consistent with the experimental emission properties in dichloromethane at room temperature. Especially, the trend experimentally observed is well respected but the calculated values are greatly underestimated by about 50 nm (only 29 nm for **2**).

The theoretical emission maxima are usually more accurate when calculated by the solvent-corrected energy difference between the DFT optimized ground and triplet states (at least when the optimized triplet state obtained in the gas phase by the use of unrestricted DFT calculations corresponds to the emissive state proposed by the TD-DFT calculations). It is clearly the case for our series of compounds since the average error is 14 nm, going from a minimum of 2 nm for **3** to a maximum of 21 nm for **1**, **4** and **6**. The emissive states are calculated to arise from the promotion of one electron from the HOMO to the LUMO for **1**, **3** and **4**, from the HOMO to the LUMO+2 for **2**, and from the HOMO-1 to the LUMO for **6** (Figure 8). After the geometry relaxation of the excited states, these closed-shell frontier orbitals were found to be the singly occupied α-HOMO and α-HOMO-1 (Figure 9) in the low-lying triplet states, except for **6** for which the singly occupied molecular orbitals involved in the emission process are found to be α-HOMO and α-HOMO-4: α-HOMO-1, α-HOMO-2 and α-HOMO-3 exhibit electron density mainly on the alkynyl ligand and the corresponding β spin orbitals can be found in the orbital diagram with similar shapes and energies. For the ppy and 5mthpy containing complexes **1**, **3**, **4** and **6**, the electron density is mainly localized on the cyclometalated ligand with a π-antibonding character between the two cycles for α-HOMO-1 (or α-HOMO-4 in **6**) and to the opposite with a π-bonding character for α-HOMO (Figure 9 for **1**). The main variation observed in the triplet state geometry with respect to the ground-state geometry is a significant shortening of the central C–C bond by 0.081 Å for **1**, 0.054 Å for **3**, 0.079 Å for **4** and 0.078 Å for **6**. Beside the related bond shortenings, elongations of the neighboring C–C and C–N bonds involving the same central carbon atoms and the metal coordinated carbon and nitrogen atoms are observed in the range of 0.056–0.097 Å. For complex **3**, the elongation of the C=C bond (reported as C1-C5 in the crystal structure **3a**, Figure 1) is more important than the shortening of the central C–C bond, +0.097 vs. −0.054 Å). In the case of **2** which contains the bzq ligand, an opposite feature is observed for the external C=C bond (reported as C12-C13 in the crystal structure, Figure 1) since α-HOMO-1 exhibits a π-bonding character of the external C=C bond and α-HOMO a π-antibonding character. Consequently, the main deviation observed in the bond lengths of the triplet state (with respect to the ground state) is a significant elongation of the former double bond by more than 0.1 Å, from 1.364 to 1.465 Å.

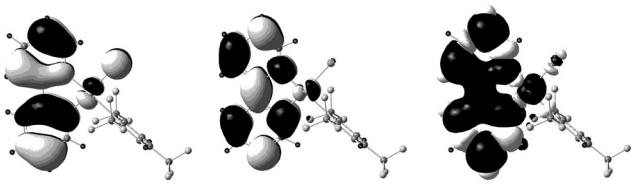

Figure 9. Spatial plots of the singly occupied α-HOMO-1 (left) and α-HOMO (middle) as well as the spin density surface (right) of the optimized triplet state of **1**, showing the ^{3}ILCT($\pi_{ppy}\rightarrow\pi^*_{ppy}$) character of the emission process.

The spin density plots, which take into account the electron density on all α and β singly occupied orbitals of the triplet states, visually identify the origin of the emission in the metallacycles showing the ^{3}ILCT($\pi_{N\wedge C}\rightarrow\pi^*_{N\wedge C}$) character of the emission process (Figure 9–11). It is worth to note that the contribution of the metal is very low, less than 3% considering the composition of the α-HOMOs of the triplet states, or less than 5% in the corresponding frontier orbitals of the ground states.

As previously detailed, emission from **7** was found to be significantly dependent on the polarity of the solvent. Obviously, intermolecular interactions between the solvent molecules and the chromophore affect the emission properties. The TD-DFT results for **7** (439.0 nm for the lowest singlet–triplet vertical excitation T_1–S_0 energy) are consequently not in agreement with the experimental emission data recorded in dichloromethane at room temperature (λ_{max} = 612 nm). Among the conditions

Figure 10. Spatial plots of the singly occupied α-HOMO−1 (left) and α-HOMO (right) as well as the spin density surface (down) of the optimized triplet state of **7**, showing the ^{3}ILCT($\pi_{alk}\rightarrow\pi^*_{alk}$) and ^{3}LLCT($\pi_{ppy}\rightarrow\pi^*_{alk}$) characters of the emission process.

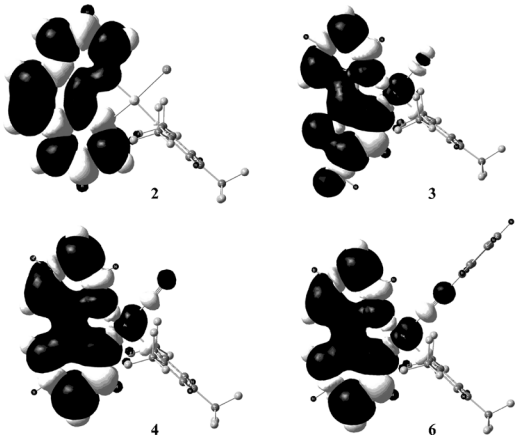

Figure 11. Spin density surfaces for the optimized triplet states of **2**, **3**, **4**, and **6**, showing the ^{3}ILCT($\pi_{N\wedge C}\rightarrow\pi^*_{N\wedge C}$) character of the emission processes.

chosen for the experimental work, 5 wt% PMMA with a low concentration of the complex (5 wt%) in a non-polar media (PMMA) seems to be the condition for which these interactions should be the most reduced. The difference of 26 nm between the calculated value of 468.0 nm and the experimental emission maximum of 494 nm (in 5 wt% PMMA) is in a better agreement and is comparable with the results obtained for the other selected complexes **1**, **2**, **3**, **4**, and **6** (Table 5). The maximum wavelength is even better estimated by the energy difference between the DFT optimized ground and triplet states with a calculated value of 490 nm: an absolute error of 4 nm for **7** which corresponds well to the error range of 2–21 nm observed for the other complexes of the series. The choice of 5 wt% PMMA as a reference for the TD-DFT calculations of **7** is justified by the fact that 1) the experimental emission maxima are very similar (±3 nm) when recorded in a solution of dichloromethane at room temperature and in a 5 wt% PMMA film for all complexes (except **7**), 2) when the concentration of **7** in PMMA increases, the emission band is redshifted (494 nm for 5 wt%, 501 nm for 25 wt%, 511 nm for 50 wt% and 523 nm for 75 wt%) tending toward the most redshifted value of 622 nm recorded in the solid state, where the intermolecular interactions are expected to be the strongest ones.

The transitions responsible of the emission band of **7** involves HOMO, LUMO+4 and LUMO+5 in the singlet state and the singly occupied α-HOMO-1 and α-HOMO (Figure 10) in the triplet state. Unlike the other complexes, these orbitals have mainly contributions from the alkyne ligand (95% in α-HOMO−1) and really less from the cyclometalated ligand (37% vs. 56% in α-HOMO-1; see the Supporting Information). The geometry of the DFT optimized triplet state confirms its origin from the promotion of one electron from HOMO to LUMO+4/LUMO+5. Indeed, the main changes observed in the triplet state geometry with respect to the ground-state geometry are seen in the alkyne ligand. The spin density surface of the optimized triplet state of **7** (Figure 10) together with the former observations reveal the different behavior of **7** in comparison with the other complexes showing the ^{3}ILCT($\pi_{alk}\rightarrow\pi^*_{alk}$) and ^{3}LLCT($\pi_{ppy}\rightarrow\pi^*_{alk}$) characters of the emission process, which is consistent with the experimental findings.

Conclusions

The synthesis and photophysical investigations of neutral Au^{III} complexes based on a new monocyclometalated structural motif of the type *cis*-[(NC)Au($C_6H_2(CF_3)_3$)(R)] is reported. The propensity for reductive elimination was successfully suppressed with the introduction of the Fmes ligand. Both steric and electronic factor favored the isolation of the only monosubstituted Fmes product in high yields. This further allowed for the successful substitution of the monochloro complex [(ppy)Au($C_6H_2(CF_3)_3$)(Cl)] with a judicious choice of the ancillary ligands resulting in complexes **4**–**7** and one among them being the first isolated and characterized *cis* aryl alkyne Au^{III} complex. These complexes were thermally stable and also displayed significantly improved luminescence efficiency both in solution and solid state. A quantum yield of 39% obtained in the case of **7** is the highest reported for a Au^{III} complex in the solid state. Complex **7** displayed a widely tunable emission behavior ranging from the deep blue region to the red region of the visible spectrum depending on the microenvironment of a single Au^{III} complex. DFT and TD-DFT calculations carried out further add support to the findings from the photophysical investigations of the complexes. The good luminescence efficiencies combined with widely tunable emission behavior and thermal stability obtained based on the monocyclometalated Au^{III} monoaryl motif makes them a promising fragment for the synthesis of highly efficient triplet phosphors for OLEDs applications.

Experimental Section

^{1}H NMR, ^{13}C NMR, ^{19}F NMR and elemental analyses; thermogravimetric analyses; absorption and emission spectra; details about DFT calculations and X-ray diffraction analyses; Lippert plot for **7** are contained in the Supporting information. CCDC-951786 (**1**), CCDC-951787 (**2**) and CCDC-951788 (**3a**), CCDC-951789 (**3b**), CCDC-951790 (**4**), CCDC-951791 (**5**), CCDC-951792 (**6**), contain the supplementary crystallographic data for this paper. These data can be obtained free of charge from The Cambridge Crystallographic Data Centre via www.ccdc.cam.ac.uk/data_request/cif.

Acknowledgements

The authors wish to thank Dr. Thomas Fox for help with NMR studies, Dr. Ferdinand Wild for TGA measurements and Prof. Heinz Berke and Prof. Roger Alberto for the generous support. Financial support from the Swiss National Science Foundation (Grant no. 200021-135488) and the University of Zurich is gratefully acknowledged.

Keywords: acetylides · charge transfer · gold · OLED · phosphorescence

[1] a) K. M.-C. Wong, X. L. Zhu, L.-L. Hung, N. Y. Zhu, V. W.-W. Yam, H.-S. Kwok, *Chem. Commun.* **2005**, 2906–2908; b) V. W.-W. Yam, K. M.-C. Wong, L.-L. Hung, N. Y. Zhu, *Angew. Chem.* **2005**, *117*, 3167–3170; *Angew. Chem. Int. Ed.* **2005**, *44*, 3107–3110; c) K. M. C. Wong, L. L. Hung, W. H. Lam, N. Y. Zhu, V. W. W. Yam, *J. Am. Chem. Soc.* **2007**, *129*, 4350–4365; d) V. K.-M. Au, K. M.-C. Wong, N. Y. Zhu, V. W.-W. Yam, *J. Am. Chem. Soc.* **2009**, *131*, 9076–9085; e) V. K.-M. Au, K. M.-C. Wong, D. P.-K. Tsang, M.-Y. Chan, N. Zhu, V. W.-W. Yam, *J. Am. Chem. Soc.* **2010**, *132*, 14273–14278; f) V. K. M. Au, K. M. C. Wong, N. Y. Zhu, V. W. W. Yam, *Chem. Eur. J.* **2011**, *17*, 130–142; g) V. K. M. Au, W. H. Lam, W. T. Wong, V. W. W. Yam, *Inorg. Chem.* **2012**, *51*, 7537–7545; h) V. K. M. Au, N. Y. Zhu, V. W. W. Yam, *Inorg. Chem.* **2013**, *52*, 558–567; i) M. C. Tang, D. P. K. Tsang, M. M. Y. Chan, K. M. C. Wong, V. W. W. Yam, *Angew. Chem.* **2013**, *125*, 464–467; *Angew. Chem. Int. Ed.* **2013**, *52*, 446–449; j) C. W. Chan, W. T. Wong, C. M. Che, *Inorg. Chem.* **1994**, *33*, 1266–1272; k) K. H. Wong, K. K. Cheung, M. C. W. Chan, C. M. Che, *Organometallics* **1998**, *17*, 3505–3511; l) W. P. To, K. T. Chan, G. S. M. Tong, C. S. Ma, W. M. Kwok, X. G. Guan, K. H. Low, C. M. Che, *Angew. Chem.* **2013**, *125*, 6780–6784; *Angew. Chem. Int. Ed.* **2013**, *52*, 6648–6652; m) W. P. To, T. Zou, R. W. Y. Sun, C. M. Che, *Philos. Trans. R. Soc. London Ser. A* **2013**, *371*, 20120126; n) X. S. Xiao, W. L. Kwong, X. G. Guan, C. Yang, W. Lu, C. M. Che, *Chem. Eur. J.* **2013**, *19*, 9457–9462.

[2] a) H. Yersin in *Highly efficient OLEDs with Phosphorescent Materials*, Wiley-VCH, Weinheim, **2008**; b) M. A. Baldo, D. F. O'Brien, Y. You, A. Shoustikov, S. Sibley, M. E. Thompson, S. R. Forrest, *Nature* **1998**, *395*,

151 – 154; c) M. A. Baldo, M. E. Thompson, S. R. Forrest, *Nature* **2000**, *403*, 750 – 753.
[3] a) J. Brooks, Y. Babayan, S. Lamansky, P. I. Djurovich, I. Tsyba, R. Bau, M. E. Thompson, *Inorg. Chem.* **2002**, *41*, 3055 – 3066; b) J. Li, P. I. Djurovich, B. D. Alleyne, M. Yousufuddin, N. N. Ho, J. C. Thomas, J. C. Peters, R. Bau, M. E. Thompson, *Inorg. Chem.* **2005**, *44*, 1713 – 1727.
[4] C. Bronner, O. S. Wenger, *Dalton Trans.* **2011**, *40*, 12409 – 12420.
[5] a) A. Herbst, C. Bronner, P. Dechambenoit, O. S. Wenger, *Organometallics* **2013**, *32*, 1807 – 1814; b) D. A. Rosca, D. A. Smith, M. Bochmann, *Chem. Commun.* **2012**, *48*, 7247 – 7249.
[6] J. A. Garg, O. Blacque, T. Fox, K. Venkatesan, *Inorg. Chem.* **2010**, *49*, 11463 – 11472.
[7] J. A. Garg, O. Blacque, K. Venkatesan, *Inorg. Chem.* **2011**, *50*, 5430 – 5441.
[8] C. Bartolomé, P. Espinet, J. M. Martin-Alvarez, F. Villafane, *Eur. J. Inorg. Chem.* **2003**, 3127 – 3138.
[9] E. Langseth, C. H. Gorbitz, R. H. Heyn, M. Tilset, *Organometallics* **2012**, *31*, 6567 – 6571.
[10] a) A. Vitérisi, A. Orsini, J. M. Weibel, P. Pale, *Tetrahedron Lett.* **2006**, *47*, 2779 – 2781; b) R. Maag, B. H. Northrop, A. Butterfield, A. Linden, O. Zerbe, Y. M. Lee, K. W. Chi, P. J. Stang, J. S. Siegel, *Org. Biomol. Chem.* **2009**, *7*, 4881.
[11] D. M. Fan, C. T. Yang, J. D. Ranford, P. F. Lee, J. J. Vittal, *Dalton Trans.* **2003**, 2680 – 2685.
[12] a) E. Z. Von Lippert, *Electrochemistry* **1957**, *61*, 962; b) N. Mataga, Y. Kaifu, M. Koizumi, *Bull. Chem. Soc. Jpn.* **1956**, *29*, 465; c) J. R. Lackowicz, *Principles of Flourescence Spectroscopy*, Plenum, NewYork, **1983**.
[13] a) P. T. Chou, Y. Chi, M. W. Chung, C. C. Lin, *Coord. Chem. Rev.* **2011**, *255*, 2653 – 2665; b) D. Kim, J. L. Bredas, *J. Am. Chem. Soc.* **2009**, *131*, 11371 – 11380.
[14] Gaussian 03 (Revision D.01), M. J. Frisch, G. W. Trucks, H. B. Schlegel, G. E. Scuseria, M. A. Rob, J. R. Cheeseman, J. A. Montgomery, Jr., T. Vreven, K. N. Kudin, J. C. Burant, J. M. Millam, S. S. Iyengar, J. Tomasi, V. Barone, B. Mennucci, M. Cossi, G. Scalmani, N. Rega, G. A. Petersson, H. Nakatsuji, M. Hada, M. Ehara, K. Toyota, R. Fukuda, J. Hasegawa, M. Ishida, T. Nakajima, Y. Honda, O. Kitao, H. Nakai, M. Klene, X. Li, J. E. Knox, H. P. Hratchian, J. B. Cross, V. Bakken, C. Adamo, J. Jaramillo, R. Gomperts, R. E. Stratmann, O. Yazyev, A. J. Austin, R. Cammi, C. Pomelli, J. W. Ochterski, P. Y. Ayala, K. Morokuma, G. A. Voth, P. Salvador, J. J. Dannenberg, V. G. Zakrzewski, S. Dapprich, A. D. Daniels, M. C. Strain, O. Farkas, D. K. Malick, A. D. Rabuck, K. Raghavachari, J. B. Foresman, J. V. Ortiz, Q. Cui, A. G. Baboul, S. Clifford, J. Cioslowski, B. B. Stefanov, G. Liu, A. Liashenko, P. Piskorz, I. Komaromi, R. L. Martin, D. J. Fox, T. Keith, M. A. Al-Laham, C. Y. Peng, A. Nanayakkara, M. Challacombe, P. M. W. Gill, B. Johnson, W. Chen, M. W. Wong, C. Gonzalez, J. A. Pople, (Gaussian, Inc., Wallingford, CT, **2003**).
[15] C. Adamo, V. Barone, *J. Chem. Phys.* **1999**, *110*, 6158 – 6170.
[16] T. H. Dunning, Jr., P. J. Hay, *Modern Theoretical Chemistry*, Plenum, New York, **1976**.
[17] R. Ditchfield, W. J. Hehre, J. A. Pople, *J. Chem. Phys.* **1971**, *54*, 724.
[18] a) R. Bauernschmitt, R. Ahlrichs, *Chem. Phys. Lett.* **1996**, *256*, 454 – 464; b) M. E. Casida, C. Jamorski, K. C. Casida, D. R. Salahub, *J. Chem. Phys.* **1998**, *108*, 4439 – 4449; c) R. E. Stratmann, G. E. Scuseria, M. J. Frisch, *J. Chem. Phys.* **1998**, *109*, 8218 – 8224.
[19] a) V. Barone, M. Cossi, *J. Phys. Chem. A* **1998**, *102*, 1995 – 2001; b) M. Cossi, N. Rega, G. Scalmani, V. Barone, *J. Comput. Chem.* **2003**, *24*, 669 – 681.
[20] J. A. Garg, O. Blacque, J. Heier, K. Venkatesan, *Eur. J. Inorg. Chem.* **2012**, 1750 – 1763.

Received: September 18, 2013
Published online on January 30, 2014

